Journal of Mineral Resources Engineering, 9(2): 1-12, (2024)

Imam Khomeini International University
Vol. 9, No. 2, Summer 2024, pp. 1-12

نشریه مهندسی منابع معدنی
Journal of Mineral Resources Engineering (JMRE)

Research Paper

Pore Space Quantification of Three Sandstones Binary Micro CT Images

Ashrafi M.[1], Tabatabaei-Nezhad S.A.[2*], Khodapanah E.[3]

1- Ph.D Student, Faculty of Petroleum and Natural Gas Engineering, Sahand University of Technology, Tabriz, Iran
2- Professor, Faculty of Petroleum and Natural Gas Engineering, Sahand University of Technology, Tabriz, Iran
3- Associate Professor, Faculty of Petroleum and Natural Gas Engineering, Sahand University of Technology, Tabriz, Iran

Received: 13 Apr. 2021 **Accepted: 12 Jul. 2021**

Abstract: The pore geometry and topology properties of rocks are significant for a better understanding of the complex hydrologic and elastic properties. If the complexity of porous media is considered, reliable results can achieve. In three-dimensional imaging of cavities, these complexities are taken into account. In this study, by conducting different methods deep understanding from some sandstones pore space is undertaken. Three series of 2D micro-computed tomography sandstones binary images have been considered, each of them imagined as a 3D binary image. Using novel skeletonization and pore-throat partitioning algorithms some network properties have been evaluated and compared for three cases. Those properties are pore and grain size distribution, throat length frequency, and coordination number frequency. Also, geometric measures in 2D and 3D have been considered using Minkowski functionals. The area, the perimeter and the 2D Euler number of 2D binary images and the volume, the surface area, the mean breadth also known as integral of the mean curvature, and the 3D Euler Number of 3D binary images are considered.

Keywords: Pore network characterization, Sandstones, 3D binary image, Skeletonization, Skeleton to graph.

How to cite this article
Ashrafi, M., Tabatabaei-Nezhad, S. A., and Khodapanah, E. (2024). *"Pore space quantification of three sandstones binary micro CT images"*. Journal of Mineral Resources Engineering, 9(2): 1-12.
DOI: 10.30479/JMRE.2021.15372.1505

*Corresponding Author Email: *tabatabaei@sut.ac.ir*

1- INTRODUCTION

Sandstone reservoirs contain wide pore throat sizes ranging and have complex pore geometry and pore throat structure. Microscopic pore throat structures are the most important factors affecting the macroscopic reservoir quality and fluid flow in tight sandstones. The importance of evaluation characterization quantitatively of the microscopic pore structures are obvious. These properties including pore geometry, pore size distribution, and pore connectivity that can help maintain and enhance petroleum recovery.

To characterize sandstones different parameters can be considered, for example, pore size distribution that can be characterized by many techniques, such as thin-section analysis, scanning electron microscopy (SEM), X-ray computed tomography (CT), pressure-controlled porosimetry (PCP), rate-controlled porosimetry (RCP), nuclear magnetic resonance (NMR) and N2 adsorption regarding these techniques all have limitations.

PCP fails to measure large pores, RCP cannot reveal the distribution of tiny throats, SEM and thin sections fail to provide quantitative data, CT is expensive while it has the inevitable error in calculating pore-throat radius, NMR test range is limited by surface relaxivity [1].

Other properties are the same in various methods. To improve the accuracy of rock characterization usage of all available methods is the best way, although there are always drawbacks, in this study only some properties will be considered to characterize three sandstones micro-CT images. It is clear that the integration of several techniques appears to be the best way for characterizing their overall pore-throat distribution.

When proper images of rocks are available then by finding the relationship between image properties and desired specification of rock, quantification will be simple in manner of indirect. Nowadays different techniques have been developed to characterize porous media [2-5]. Among these methods micro-computed tomography known as micro-CT imaging is one of the most referred [6].

Assuming what is considered to be a pore and/or throat, a pore network can be constructed directly from images. The closer to the real porous media, the better network. Pore network robustness depends on the way of partitioning the real void space to pore and throat [7]. Also, the location, size, and shape of pores and throats influence network properties.

There are three void space representation methods that can help better porous characterization [8]. First is the creation by consideration of sedimentary process in which the rock is formed, second is statistically equivalent network generation using distributions of basic morphologic parameters and third is direct micro-CT imaging from a real sample to yield an irregular lattice [9].

To get a researcher more details about pore spaces network, selection of image analysis techniques is essential [7]. The medial axis-based algorithms create an image skeleton. Throats are located at local minima and pores are at the skeleton nodes [10,11]. Skeleton properties also can bring more details of pores and throats.

Pore topology has great importance so standard parameters can be used to characterize pore space. Standard parameters used in quantitative analysis of spatial structures are area, perimeter in 2D, volume, surface area and mean breadth in 3D. Another parameter is the Euler-Poincaré characteristic, these parameters from the so-called Minkowski functionals can be evaluated. The Euler-Poincaré characteristic is a standard connectivity parameter, for a planar structure, it is equal to the number of its connected components minus its number of holes [12].

Euler number (χ) depends on vertices (V), edges (E), faces (F), or solids (S) numbers (#) of the reconstruction as Equation 1 which is classical Euler formula.

$$\chi = \#\mathrm{V} - \#\mathrm{E} + \#\mathrm{F} - \#\mathrm{S} \quad (1)$$

The approximation of the Euler-Poincaré measure strongly depends on the choice of the adjacency system. Different adjacencies can yield very different results. One possibility is to choose the adjacency depending on the geometry of the structure. For example, one can choose

4-adjacency or 6-adjacency for thick structures, and 8-adjacency or 26-adjacency for structures presenting thin edges.

1-1- Permeability from geometric and topological properties

If characterization is conducted well on samples then petro physical properties can be achieved by help of properties derived during characterization. For example, a review of methods considering geometric or topological properties to get absolute permeability is described in the following paragraphs.

Absolute permeability represents the ability of a porous medium to conduct fluid flow. It is usually measured through a core flooding experiment and calculated from Darcy's Law as Equation 2.

$$K = \frac{Q\mu L}{A\Delta \mathrm{P}} \tag{2}$$

Where:
K: absolute permeability,
Q: flow-current,
μ: fluid viscosity,
L: the length of the sample,
A: cross-sectional area,
ΔP: is pressure gradient.

The Carman-Kozeny equation is a well-known empirical equation where permeability is dependent on rock porosity, which can be seen in Equation 3.

$$K = \frac{\phi r^2}{8\tau} \tag{3}$$

Where:
ϕ: rock porosity,
r: effective radius,
τ: is tortuosity.

A commonly used approximate permeability-porosity relation is the Kozeny-Carman equation also is expressed as Equation 4.

$$K = \frac{1}{72}\frac{\phi^3}{(1-\phi)^2}\frac{1}{\tau^2}D^2 \tag{4}$$

Where:
D: is grain diameter.

This model assumes that a porous medium can be represented as a solid block permeated by parallel cylindrical pipes. The proportionality constant 1/72 is sometimes replaced with a fitting parameter.

Another widely used empirical correlation is the Katz-Thompson model as shown below.

$$K = cl_c{}^2\frac{\sigma}{\sigma_0} \tag{5}$$

Where:
c: the constant on the order of 1/226,
lc: the characteristic length of the pore space,
σ: is the conductivity of rock saturated with a brine solution of conductivity σ_0.

Because electrical conductivity is influenced by the topology of the pore space this relationship implicitly captures pore topology while the geometry of the pore space is captured through the characteristic length term. The σ/σ_0 term can be linked to porosity according to Archie's law as shown below.

$$\frac{\sigma}{\sigma_0} = \frac{(\phi-\phi_c)^z}{(1-\phi_c)} \tag{6}$$

Where:
ϕ_c: porosity at the percolation threshold,
z: is the critical exponent.

The Katz-Thompson model has been further developed by replacing the σ/σ_0 term with direct measurements of pore morphology. The new formulated equation is shown in Equation 7 and we will be referred to it as Scholz's model from hereon.

$$K = cl_c{}^2(\frac{1-\chi_0}{N})^\alpha \tag{7}$$

Where:
χ_0: is the Euler characteristic of the conducting phase,
N: is the number of grains in the granular porous media.

For a 2D geometry c=1/12 and α is a free parameter that best agreement is found for α=1.27.

Scholz proposed to replace effective grain number by N as below [13].

$$\widehat{N} = \frac{P^2}{4\pi A\phi} - \frac{\chi}{\phi} \quad (8)$$

Where:
P: perimeter,
A: is area.

Conceptual models for prediction of 3D permeability of the Lattice Boltzmann from computed 2D permeabilities presented by Saxena. No single approach can yield perfect 2D-to-3D transforms, since this problem is fundamentally non-unique given that the same 2D microstructure can be cut from many different 3D composites. Saxena proposed two models, the Kozeny-Carman approach (Model 1) and the flow path deviation approach (Model 2) [14].

In the first model, the Kozeny-Carman expression for permeability can also be expressed as Equation 9.

$$K \approx \frac{1}{2}\frac{\phi^3}{\tau^2 {S_0}^2} \quad (9)$$

Where:
S_0: is the specific surface area.

So one can write Equation 10.

$$\frac{K_{3D}}{K_{2D}} \approx \frac{S_{2D}^2}{\tau_{3D}^2 S_{3D}^3} \quad (10)$$

For an arbitrary packing of identical spherical grains in 3D, the specific surface area is $S_{3D} = 3(1 - \phi)/R$, where R is the sphere radius. Similarly, the specific surface area for an arbitrary packing of parallel circular cylinders is $S_{2D} = 2(1 - \phi)/R$, where R is the cylinder radius.

Saxena used a model for porosity dependent tortuosity as Equation 11.

$$\tau_{3D} \approx 1 - plog\phi \quad (11)$$

Where:
p: is an empirical parameter (p = 0.41 for sphere packs; p = 0.63 for cubes).

Therefore, the estimated 3D permeability is given by Equation 12 [14].

$$K_{3D} \approx \frac{4}{9}\frac{K_{2D}}{(1 - plog\phi)^2} \quad (12)$$

Model 1 does not incorporate the effects of change in flow field from pipes of fixed diameter in 2D to variable diameter in 3D. Thus, Saxena considered another approach that accounts for sinusoidally changing pore diameter in 3D along with distortion of pipe diameter upon slicing. The final expression for model 2 is given by Equation 13 [14].

$$K_{3D} \approx 0.24\frac{1}{1-\bar{\delta}}\ {}^4\!2\left(1-\bar{\delta}^2\right)^{\frac{7}{5}}\frac{}{2+3\bar{\delta}^2}\left(1+\frac{16\pi^2}{3}\frac{\bar{\delta}^2}{\bar{\lambda}^2}\frac{(1-\bar{\delta}^2)}{2+3\bar{\delta}^2}\right)^{-1}K_{2D} \quad (13)$$

Where:
$\bar{\delta}$: the normalized magnitude of variation in radius,
$\bar{\lambda}$: is the variation wavelength.

The factor 0.24 accounts for distortion of tube diameter upon slicing in all possible directions.

Model parameters p and δ depend on the details of rock microstructure. It is found that parameters p and δ sharply decline with an increase in porosity, and are well described by the following empirical relations.

$$\mathrm{p} = 3\mathrm{e}^{-7\phi} \quad (14)$$

$$\delta = \mathrm{e}^{-9\phi} \quad (15)$$

From the above equations, the dependency of topological and geometrical properties to petro physical properties is obvious as have been studied by different scholars. The purpose of this study is not to investigate petro physical properties evaluation such as absolute permeability and is the only characterization of three sandstones from their micro-CT binary images. While the importance of porous media quantification and evaluation of geometric properties is obvious from mentioned equations that show their dependency on permeability.

The novelty of the conducted study is rational petro physical and topological micro-sample porous media property evaluation. Sometimes large size plug or core samples are not available. In these situations, that there is a small piece of porous material, by using proper image acquisition methods following in the next chapter,

great understanding data can be obtained. These methods are the combination of topological Minkowski functionals and newly proposed pore network extraction methods

2- METHODS

Different type of direct imaging methods is available to describe rock materials. Micro-CT imaging is an accurate and repeatable method of evaluating the pore system and can be conducted on the plug, core, sidewall core, drill cuttings, and outcrop.

However, despite large amount of information available, the actual three-dimensional grain relationships and details of the intergranular pore structure were always beyond our reach. While digital image analysis is not new, important recent advances are available in petrography include pattern recognition and pattern classification software for description and quantification of rock geometric characteristics. These approaches started by development of the arena of pore image analysis to determine the size, shape, and relative proportions of different pore types through computer-based thin-section porosity analysis. It is possible to define many variables for each field of view using this technique. It is far beyond the scope of this review to even begin an analysis of the applications of image analysis to geological samples. However, in the context of analyzing and quantifying pore structures some discussion is appropriate.

A key requirement of many forms of pore structure image analysis is that they require binary images showing pore and grain space. These are typically obtained by thresholding greyscale.

Note that even for a simple system the process of image segmentation does not necessarily yield a unique solution. There are several reasons for this. First, the background, considered here as the grey-scale level may not be flat across the image. This is often a function of the instrument settings and must be corrected before thresholding/ segmentation. More importantly, however, even within a given grain there are often variations in grey-scale level, adding to the noise level.

Selecting the appropriate method for segmenting an image, either for simply choosing a threshold for a 2D or 3D image, the grey-level between the two phases, or using a more complex segmentation approach, is so important. Given the complexity of this issue, a careful examination and comparison of the various approaches clearly beyond the scope of this review while it's important to consider that there are a very large number of algorithms for selecting a threshold.

2-1- Skeleton and skeleton to graph calculation

Here, 1-voxel of a binary image is assigned to void spaces while 0-voxel for grains. By usage of skeletonization algorithm and skeleton to graph algorithm that claimed can distinguish pores and throats for a 3D binary skeleton pore properties of sandstones micro-CT images are achieved. A new skeletonization algorithm and skeleton to graph algorithm was proposed by Kollmannsberger [15,16]. The methods need two inputs, a 3D binary matrix and a threshold for the minimum length of branches, to filter out skeletonization artifacts. The threshold is considered one in all network extraction studied in this article. A pore network can be built by the combination of skeletonization and skeleton to graph algorithms, the pore size distribution, throat length frequency, and coordination number for the network can be evaluated. Also, grain size distribution can be obtained by the method proposed by Rabbani [17].

Several methods can be employed to directly measure rock properties for example rock porosity can be measured directly by saturation or imbibition, buoyancy, gas expansion, gas adsorption, and mercury intrusion porosimetry. All five of these methods only measure the effective porosity of the rock sample. By micro-CT image consideration, all types of porosities can be considered.

2-2- Geometric properties calculation

The Minkowski geometric measures for 2D images parameters are the area, the perimeter, and the (2D) Euler Number and for 3D images parameters are the volume, the surface area (called surface), the mean breadth (also known as integral of mean curvature) and the (3D) Euler Number [12].

The area of the object in a binary image

corresponds roughly to the total number of pixels in the image, but may not be the same because different patterns of pixels are weighted differently. An algorithm estimates the area of all of the on pixels in an image by summing the areas of each pixel in the image. A single-pixel surrounded by off pixels has a total area of 1. The number of objects is the number of connected components (objects) in the binary image. Connectivity of 4 and 8 for two dimensions; 6, 18, and 26 for three dimensions can be considered.

The Euler number for the 2D binary image is a scalar whose value is the total number of objects in the image minus the total number of holes in those objects. 4-connected objects and 8-connected objects can be considered. A pixel is a part of the perimete if it is nonzero and is connected to at least one zero-valued pixel. The connectivity can be 4 or 8 for two dimensions, 6 or 18 or 26 for three dimensions [12].

3- RESULTS AND DISCUSSION

3-1- Studied cases

For three sandstones named Sandstone-1, Sandstone-2, and Sandstone-3 [18,19], micro-CT binary images network properties are investigated. For each case series of 2D images that create a 3D image are available. One slice of each case is depicted in Figure 1 and simple 3D visualization of three sandstones are depicted in Figure 2. After void and grain space pore segmentation, pore properties can be achieved, the results of the first layer separated grain size are shown in Figure 3. All cases have the same size equal 300×300×300 and approximately the same resolution as Table 1. Porosity and absolute permeability are also available in Table 1. Sandstone-1 porosity and permeability are smaller than the other two. As Figure 3, Sandstone-2 and Sandstone-3 are the same, Sandstone-1 has bigger grains and voids. Sandstone-1 pore number and throat number are lower than others. The 3D void space segmented sandstone image is shown in Figure 4.

3-2- Skeleton and graph properties

The Skeletons were converted to network graphs so all pores and throats characterization have been obtained with the algorithm proposed by Kollmannsberger [15,16]. As Mostaghimi and coworkers in 2012, image size of 200 voxels for all cases had been considered, so studied porous media was reduced to cube size of 200 voxels because 200 is Representative Elementary Volume (REV) [20]. Pore size coordination number and

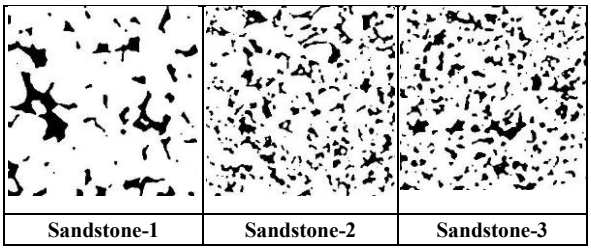

Figure 1. Sandstone first layer binary images, white color for grain and black for void space

Table 1. Sandstone sample images and petrophysics properties [18,19]

Name	Sandstone-1	Sandstone-2	Sandstone-3
Permeability (mD)	1374	4006	4555
Porosity (Fraction)	0.14	0.17	0.17
Resolution (Micron/Voxel)	8.643	9.1	8.96

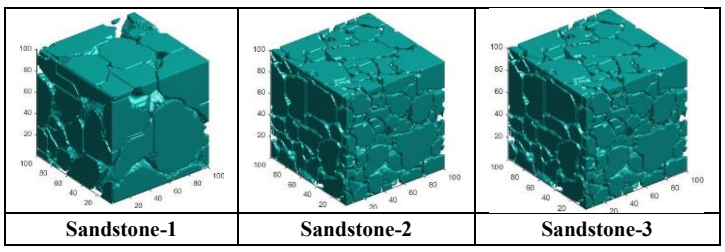

Figure 2. Simple 3D visualization of sandstone images

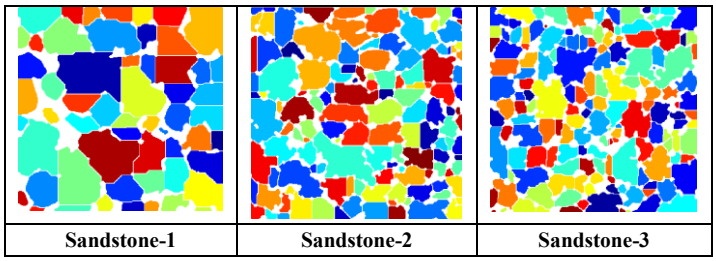

Figure 3. Sandstones first layer separated grain size after void space segmentation

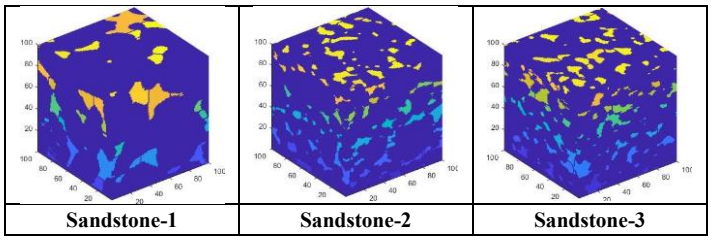

Figure 4. 3D void space segmented sandstone images

Table 2. Pore space properties of sandstone samples

Name	Sandstone-1	Sandstone-2	Sandstone-3
Region Number	122	566	902
Skeleton Porosity	0.002971	0.008302	0.008027
Biggest Pore Size (Voxel)	120	233	884
Second Big Pore Size (Voxel)	75	140	376
Third Big Pore Size (Voxel)	61	124	373
Average Pore Radius (micron)	1.7339	2.1468	2.4041
Pores Number	3171	8941	8719
Average Coordination Number	2.0195	2.2469	2.08
Maximum Coordination Number	18	10	18
Throats Number	3202	10045	9068
Average Throats Length (micron)	7.5712	6.6445	6.6971
Maximum Throat Length (micron)	56	30	42
Average Grain Radius (micron)	162.56	104.74	96.07

throat length frequencies for each network have been obtained. Largest pore size, average pore size, pores number, throats number, average throat length, maximum throat length, average coordination number, and maximum coordination number for all cases have been determined as Table 2 so better sample characterization is achieved.

After partitioning void space as nodes and links as Kollmannsberger [15,16], throat lengths specification will be clear from links properties. Pore size distribution is obtained by skeleton nodes evaluation and binary images Euclidean distance transform; from this, each pore volume is attained. Pore and grain size distribution is depicted in Figure 5.

The pore network for each case is shown in Figure 6 as the method introduced by Rabbani [17]. To show the size of sphere pores and throat

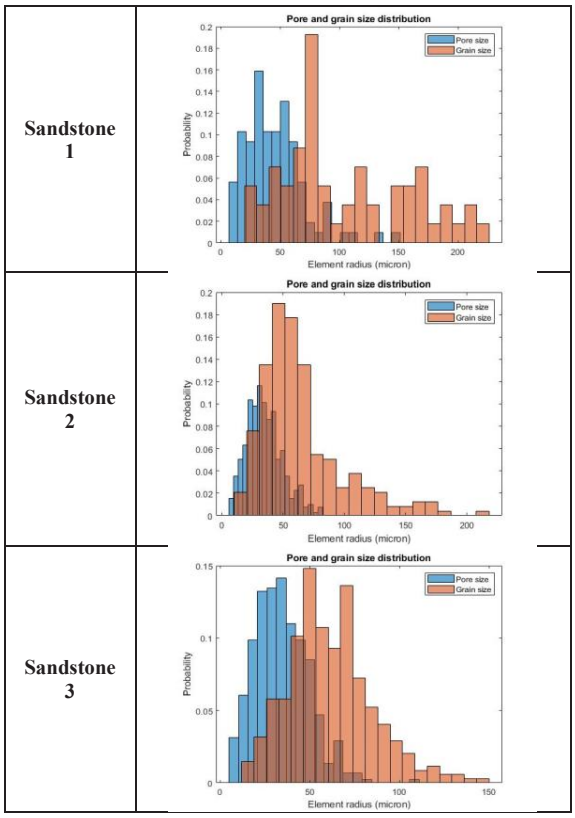

Figure 5. Pore and grain size distribution for three sandstone

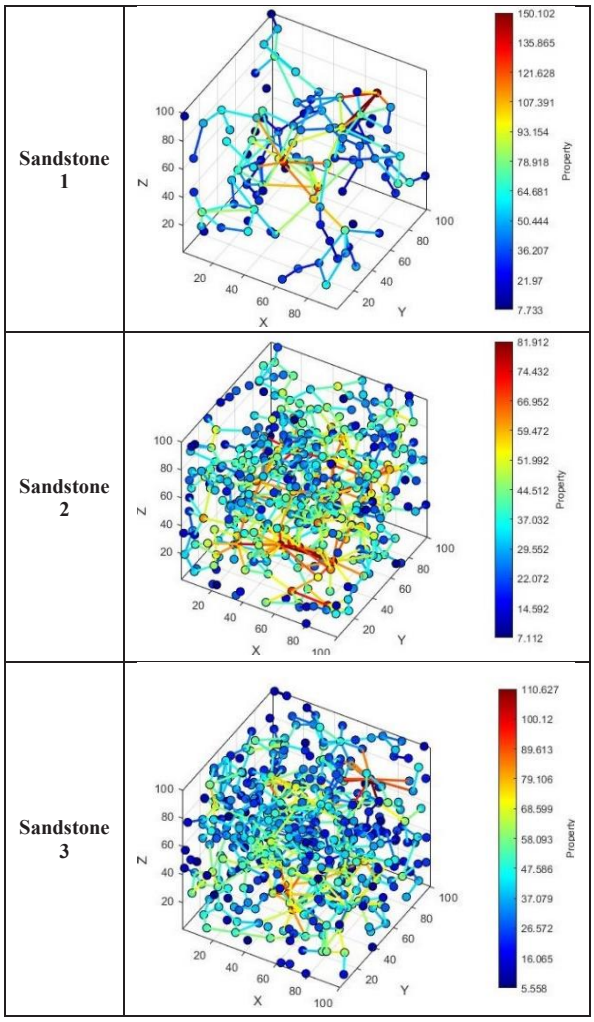

Figure 6. Pore network of three sandstones, pore and throat size are shown by color

lines length, a color bar is used that shows red for the largest sphere and blue for the smallest ones. As Figure 6 is shown, the sandstone-1 pore network is thin because of lower pore and throat number and as a result of lower porosity and permeability. Throat length frequency curves are depicted in Figure 7.

3-3- Samples grain size

Grain size distribution can be evaluated by the method proposed by Rabbani [17]. When Rabbani's method to segment grain space applies to 3D images depicted in Figure 2 then grain size distribution for all three cases are as Figure 5. The average grain radius for all cases is available in Table 2. Sandstone-1 average grain size is higher than others. In anywhere in this article Rabbani's method [17] has been used, 100×100×100 images are considered.

3-4- Sample Minkowski functionals

To see geometric properties of sandstones calculation of Minkowski functional for three

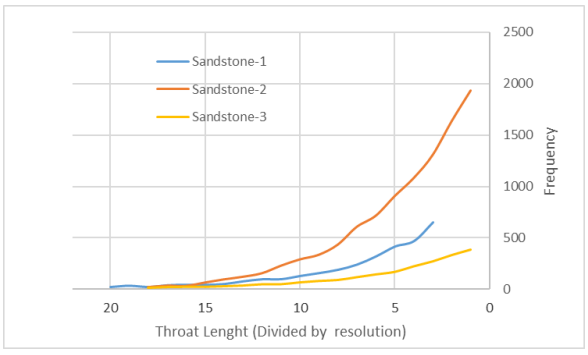

Figure 7. Sandstone networks throat length frequency

cases are conducted and stabilized in Table 3. Area, perimeter, Euler number, and number of objects for 2D images and volume, surface, mean breadth, Euler number, and several objects for 3D images for all possible connectivity are obtained. As Table 3 all 2D and 3D properties of Sandstone-1 except 3D Euler number are lower than others, So roughly more permeability higher 2D and 3D geometric properties. For each 2D binary layer of cases porosity, Euler number, area, and perimeter are calculated and their frequencies are depicted in Figures 8, 9 and 10 respectively. 2D properties frequency of Sandstone-2 and Sandstone-3 are approximately the same for all four investigated parameters that again emphasize their petro physical behavior should be the same.

3-5- Concise Results

For three sandstone micro-CT image pore network, pore and throat and grain properties were evaluated and depicted in mentioned figures. Properties variation have been shown that low porosity sample has lower pore number, pore size, throat number, and skeleton porosity, and that has higher grain size.

Also, geometrical properties such as perimeter, area, and Euler number for each 2D layer of the 3D image are studied, as a result, higher those properties mean more permeability.

Not exist proper experimental data for permeability and porosity, as the most important petro physical properties, because the size of porous media cases is very small and experimental methods can't be applied. Other measurements of image evaluated from the calculation on the binary image are exact and only numerical errors arise during computations due to round-off errors and truncation errors are irreducible.

4- CONCLUSION

In the conducted study using skeletonization and skeleton to graph algorithms void spaces properties of three sandstones, micro-CT binary images are characterized. Pores and grain size and throats length of three cases were obtained. Grain properties, 2D and 3D geometric properties are calculated and compared. Sandstones petrophysical behavior depends on void space topology and different factors such as pore, throat,

Table 3. Geometric parameter values of sandstone samples

Parameter	Sandstone-1	Sandstone-2	Sandstone-3
2D area	949997	1256338	1237394
2D perimeter of 2 connectivity	32978.23	68042.81	68184.81
2D perimeter of 4 connectivity	33075.37	67894.26	68102.85
2D Euler number of 4 connectivity	64.64333	231.7167	249.75
2D Euler number of 8 connectivity	64.40667	224.99	244.32
2D number of objects of 4 connectivity	65.83333	234.3	253.5733
2D number of objects of 8 connectivity	65.61333	228.0433	248.69
3D Volume	2.46E+09	3.43E+09	3.33E+09
3D surface of 3 paths	1.21E+08	2.72E+08	2.68E+08
3D surface of 13 paths	1.22E+08	2.73E+08	2.69E+08
3D mean breadth of 3 path	204484.7	830390.2	860082.3
3D mean breadth of 13 path	210264.6	834983.5	866436.9
3D Euler number of 6 connectivity	-547	-2878	63
3D Euler number of 26 connectivity	-1051.75	-6276.25	-3089.5
3D number of objects of 6 connectivity	476	3755	4039
3D number of objects of 18 connectivity	397	2494	2969
3D number of objects of 26 connectivity	385	2288	2780

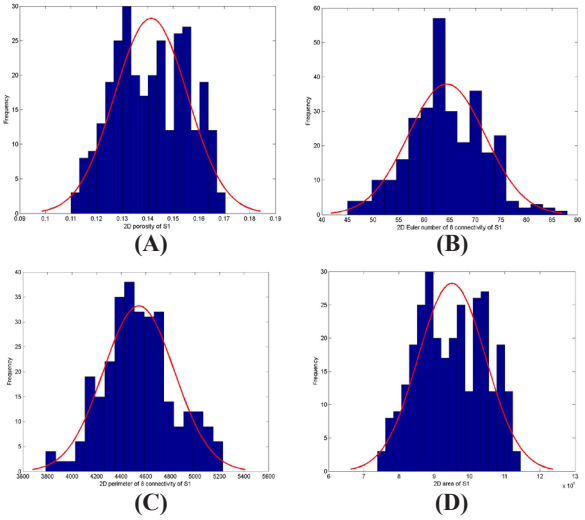

Figure 8. A: 2D porosity, B: Euler number, C: perimeter, and D: area frequencies of Sandstone-1

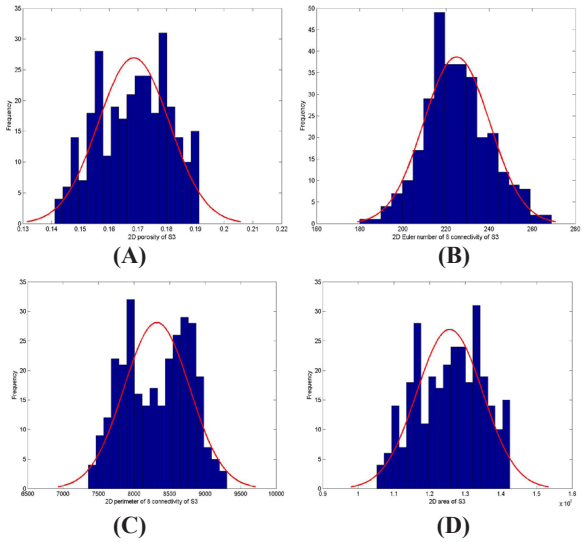

Figure 9. A: 2D porosity, B: Euler number, C: perimeter, and D: area frequencies of Sandstone-2

and grain properties should be considered to characterize them well. Geometric properties also can add more information about void space could help better characterization.

Despite different porosity and average grain radius, all the sandstone samples have approximately the same pore network and geometric frequencies trends. The high porosity sandstones exhibit wider ranges of pore sizes than the low porosity sandstone. The pore topological

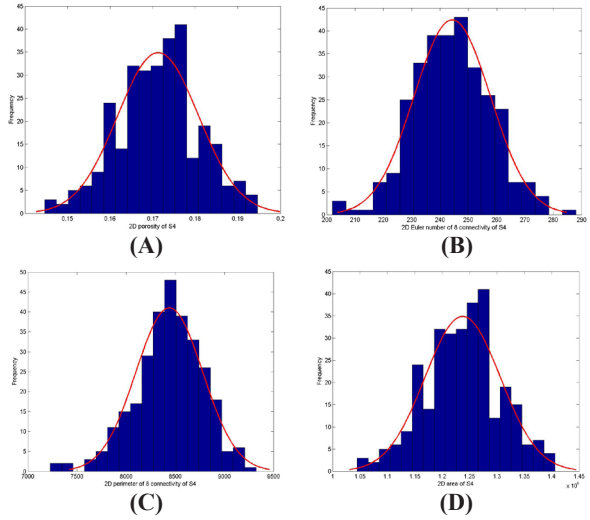

Figure 10. A: 2D porosity, B: Euler number, C: perimeter, and D: area frequencies of Sandstone-3

properties of sandstones show a high dependence on porosity. The high porosity sandstones obtain large coordination numbers, large connectivity, and lower grain size. If size and resolution be the same then higher porosity and permeability sandstone have a higher average grain radius and higher geometric properties and lower pore and throat numbers.

5- REFERENCES

[1] Lawrence, M. A., and David, R. C. (2015). *"Characterization and analysis of porosity and pore structures"*. Reviews in Mineralogy and Geochemistry, 80(1): 61-164.

[2] Gao, Z., Yang, X., Hu, C., Wei, L., Jiang, Z., Yang, S., Fan, Y., Xue, Z., and Yu, H. (2020). *"Characterizing the pore structure of low permeability Eocene Liushagang Formation reservoir rocks from Beibuwan Basin in northern South China Sea"*. Marine and Petroleum Geology, 99: 107-121.

[3] Hu, Q., Zhang, Y., Meng, X., Li, Z., Xie, Z., and Li, M. (2017). *"Characterization of micro-nano pore networks in shale oil reservoirs of Paleogene Shahejie Formation in Dongying Sag of Bohai Bay Basin, East China"*. Petroleum Exploration and Development, 44: 720-730.

[4] Kibria, M. G., Hu, Q., Liu, H., Zhang, Y., and Kang, J. (2018). *"Pore structure, wettability, and spontaneous imbibition of Woodford Shale, Permian Basin, West Texas"*. Marine and Petroleum Geology, 91: 735-748.

[5] Shao, X., Pang, X., Li, Q., Wang, P., Chen, D., Shen, W., and Zhao, Z. (2016). *"Pore structure and fractal characteristics of organic-rich shales: A case study of the lower Silurian Longmaxi shales in the Sichuan Basin, SW China"*. Marine and Petroleum Geology, 80: 192-202.

[6] Bartels, W. B., Rücker, M., Boone, M., Bultreys, T., Mahani, H., and Berg, S. (2019). *"Imaging spontaneous imbibition in full Darcy-scale samples at pore-scale resolution by fast X-ray tomography"*. Water Resources Research, 55: 7072-7085.

[7] Xiong, Q., Jivkov, A. P., and Ahmad, S. M. (2016). *"Modelling reactive diffusion in clays with two phase-informed pore networks"*. Applied Clay Science, 119: 222-228.

[8] Al-Kharusi, A. S., and Blunt, M. J. (2007). *"Network extraction from sandstone and carbonate pore space images"*. Journal of Petroleum Science and Engineering, 56(4): 219-231.

[9] Piri, M., and Blunt, M. J. (2005). *"Three-dimensional mixed-wet random pore-scale network modeling of two-and three-phase flow in porous media. I. Model description"*. Physical Review E, 71(2): 026301.

[10] Jiang, Z., Wu, K., Couples, G., van Dijke, M. J., Sorbie, K. S., and Ma, J. (2007). *"Efficient extraction of networks from three-dimensional porous media"*. Water Resources Research, 43(12): W12S03.

[11] Prodanović, M., Lindquist, W., and Seright, R. (2006). *"Porous structure and fluid partitioning in polyethylene cores from 3D X-ray microtomographic imaging"*. Journal of Colloid and Interface Science, 298(1): 282-297.

[12] Legland, D., Kieu, K., and Devaux, M. (2007). *"Computation of Minkowski measures on 2D and 3D binary images"*. Image Analysis and Stereology, 26(2): 83-92.

[13] Scholz, C., Wirner, F., Klatt, M., Hirneise, A., Schroder-Turk, G. E., Mecke, K., and Bechinger, C. (2015). *"Direct relations between morphology and transport in Boolean models"*. Physical Review E, 92(4): 043023. DOI: https://doi.org/10.1103/PhysRevE.92.043023.

[14] Saxena, N., Mavko, G., Hofmann, R., and Srisutthiyakorn, N. (2017). *"Estimating permeability from thin sections without reconstruction: Digital rock study of 3D properties from 2D images"*. United Kingdom. DOI: https://doi.org/10.1016/j.cageo.2017.02.014.

[15] Kollmannsberger, P. (2018). *"Skeleton3D, MATLAB Central File Exchange"*. Url: https://www.mathworks.com/matlabcentral/fileexchange/4-400-skeleton3d [Retrieved December 5, 2018].

[16] Kollmannsberger, P. (2018). *"Skel2Graph3D, MATLAB Central File Exchange"*. Url: https://www.mathworks.com/matlabcentral/fileexchange/43527-skel2graph-3d [Retrieved December 5, 2018].

[17] Rabbani, A., Jamshidi, S., and Salehi, S. (2014). *"Determination of Specific Surface of Rock Grains by 2D Imaging"*. Journal of Geological Research, 2014(2): 1-7.

[18] Dong, H. (2008). *"Micro-CT imaging and pore network extraction"*. Ph.D, Department of Earth Science and Engineering, Imperial College London.

[19] Raeini, A. Q., Blunt, M. J., and Bijeljic, B. (2012). *"Modelling two-phase flow in porous media at the pore scale using the volume-of-fluid method"*. Journal of Computational Physics, 231(17): 5653-5668.

[20] Mostaghimi, P., Bijeljic, B., and Blunt, M. J. (2012). *"Simulation of flow and dispersion on pore-space images"*. SPE Journal, SPE Annual Technical Conference and Exhibition, Florence, Italy, 1131-1141.

نشریه مهندسی منابع معدنی
Journal of Mineral Resources Engineering (JMRE)

دانشگاه بین المللی امام خمینی
IMAM KHOMEINI INTERNATIONAL UNIVERSITY

دوره نهم، شماره ۲، تابستان ۱۴۰۳، صفحه ۱ تا ۱۲
Vol. 9, No. 2, Summer 2024, pp. 1-12

علمی-پژوهشی

کمی‌سازی فضای خالی سه ماسه‌سنگ به وسیله تصاویر دوگانه میکرو سی تی اسکن آن‌ها

محمد اشرفی[۱]، سید علیرضا طباطبائی نژاد[۲*]، الناز خداپناه[۳]

۱- دانشجوی دکتری، دانشکده نفت و گاز، دانشگاه صنعتی سهند تبریز، تبریز
۲- استاد تمام، دانشکده نفت و گاز، دانشگاه صنعتی سهند تبریز، تبریز
۳- دانشیار، دانشکده نفت و گاز، دانشگاه صنعتی سهند تبریز، تبریز

دریافت: ۱۴۰۰/۰۱/۲۴ پذیرش: ۱۴۰۰/۰۴/۲۱

چکیده

به دست آوردن خواص هندسی و پیکربندی محیط متخلخل برای شناخت بهتر سنگ‌ها کمک فراوانی می‌کند. فضای متخلخلی از سنگ که به وسیله عکس‌های سه‌بعدی به دست آید نیز نتایج قابل اعتمادی را مشخص می‌کند. در این مقاله با اعمال روش‌های مختلف شناخت کاملی از فضای خالی سه نمونه ماسه‌سنگ به دست آمده است. ابتدا سه سری از عکس‌های دوبعدی میکرو سی تی اسکن جمع‌آوری شده که هر سری را می‌توان به عنوان یک عکس سه بعدی نیز در نظر گرفت، سپس با استفاده از روش‌های جدید اسکلت‌سازی و جداسازی گلوگاه از منفذ پارامترهای مربوط به شبکه منافذ سه نمونه به دست آمده و مقایسه شده است. این خواص شامل فراوانی طول گلوگاه، توزیع اندازه منافذ و دانه‌ها و فراوانی عدد کئوردیناسیون است. همچنین اندازه‌های هندسی شامل سطح، محیط و عدد اویلر برای عکس‌های دوگانه دوبعدی و حجم، سطح، میانگین پهنا و عدد اویلر برای عکس‌های سه‌بعدی دوگانه به دست آمده است.

کلمات کلیدی

مدلسازی شبکه منافذ، ماسه‌سنگ، عکس‌های دوگانه، اسکلت‌سازی، تبدیل اسکلت به گراف.

استناد به این مقاله
اشرفی، م.، طباطبائی نژاد، س. ع.، خداپناه، ا.؛ ۱۴۰۳؛ "کمی‌سازی فضای خالی سه ماسه‌سنگ به وسیله تصاویر دوگانه میکرو سی تی اسکن آن‌ها". نشریه مهندسی منابع معدنی، دوره نهم، شماره ۲، ص ۱۲-۱.

DOI: 10.30479/JMRE.2021.15372.1505

* نویسنده مسئول و عهده دار مکاتبات Email: tabatabaei@sut.ac.ir